Inorganic Chemistry

Supramolecular Assemblies in Silver Complexes: Phase Transitions and the Role of the Halogen Bond

Giulia Bonfant, Matteo Melegari, Davide Balestri, Francesco Mezzadri, Vittoria Marzaroli, Irene Bassanetti, and Luciano Marchiò*

Cite This: https://dx.doi.org/10.1021/acs.inorgchem.0c00256 Read Online

ACCESS | Metrics & More | Article Recommendations | Supporting Information

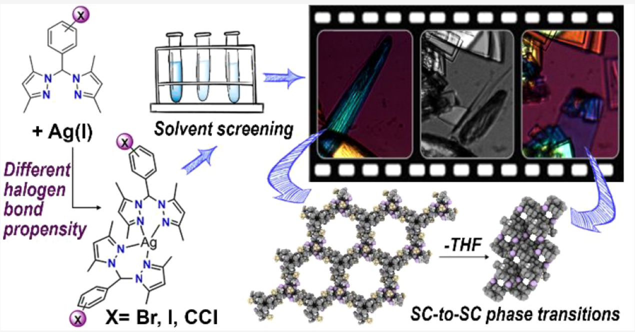

ABSTRACT: Weak interactions (hydrogen bonds, halogen bonds, CH⋯π and π−π stacking) can play a significant role in the formation of supramolecular assemblies with desired structural features. In this contribution, we report a systematic investigation on how a halogen bond (XB) can modulate the structural arrangement of silver supramolecular complexes. The complexes are composed of X-phenyl(bispyrazolyl)methane (X = Br, I) and I-alkynophenyl(bispyrazolyl)methane ligands functionalized in meta (L^{3Br}, L^{3I}) and para (L^{4Br}, L^{4I}, L^{4CCI}) positions on a phenyl ring with the purpose of providing different directionalities of the X function with respect to the N,N coordination system. The obtained $[Ag(L)_2]^+$ moieties show remarkable geometric similarities, and the L^{4Br}, L^{4I}, and L^{4CCI} ligands exhibit the most conserved types of supramolecular arrangement that are sustained by XB. The increased σ-hole in L^{4CCI} with respect to L^{4I} leads to an occurrence of short (and strong) XB interactions with the anions. $[Ag(L^{4I})_2]PF_6$ and $[Ag(L^{4I})_2]CF_3SO_3$ are characterized by the presence of three different phases, and the single-crystal evolution from phase-1 (a honeycomb structure with large 1D cavities) to phase-3 (solventless) occurs by a stepwise decrease in the crystallization solvent content, which promotes an increase in XB interactions in the lattice. The present paper aims to provide useful tools for the selection of appropriate components for the use of coordination compounds to build supramolecular systems based on the halogen bond.

■ INTRODUCTION

There is extreme variability in the 1D, 2D, and 3D structural architectures that can be built by combining metal centers and ligands with various functional groups.[1−4] In many cases, these architectures are characterized by properties that depend on structural cavities that can encapsulate additional components such as solvent molecules, counterions, and small molecules.[3,5−7] Furthermore, these architectures have applications in luminescent materials[8,9] and magnetic materials.[10,11] The presence of metal centers is also a source of potential reactivity toward the interaction and activation of small molecular guests,[12,13] and the formation of channels favors transport to and from the reactive metal centers. Moreover, structural organization in a solid state may result in a close proximity of specific molecular components, which can be made to react by external stimuli, such as UV light, to form covalent bonds that are otherwise difficult to obtain.[14−16] In many cases, the ligand is characterized by bridging functionalities; hence it is capable of linking two, or more, metal centers in an extended network. However, multidimensional architectures can be built by combining coordination compound assemblies, which may be connected due to weak interactions,[17,18] such as hydrogen bonds,[9,19−21] halogen bonds,[22,23] and π−π stackings.[24,25] For example, dimerization of carboxylic functional groups form hydrogen bond (HB) dimers,[26−28] which represent a route for expanding the dimensionality of these architectures.

In the present work, we wish to investigate the formation of supramolecular architectures formed by silver bis(pyrazolyl)methane complexes functionalized with halogen atoms such as bromine and iodine (L^{3Br}, L^{3I}, L^{4Br}, L^{4I}, L^{4CCI}, Schemes 1 and 2). The rationale behind the present work is to generate supramolecular architectures by exploring different types of covalent and noncovalent interactions, particularly halogen bonds.[29] The halogen bond is a weak interaction that has been extensively investigated in recent decades,[30−35] and it occurs due to the presence of a partial positive charge (σ hole, Cl < Br < I) on the opposite side of the σ bond.[36,37] Halogen bond interactions have been used to sustain the formation of multidimensional networks based on coordination compounds as repetitive units.[38−43] To compare the influence of halogen atoms on the structural outcome, we investigate a parent

Received: January 24, 2020

Scheme 1. (a) Previously Reported Supramolecular Architecture Based on a Ag−S Coordination and (b) an Example of a Molecular Crystal Obtained by Exploiting Halogen Bonds and Other Weak Interactions, As Reported in This Work

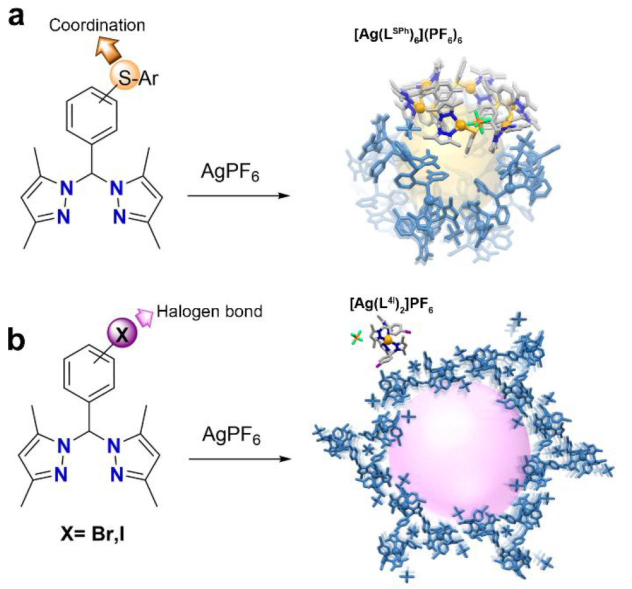

Scheme 2. (a) Bis-pyrazolyl Ligands Used in the Present Study and (b) a Summary of the Complexes Synthesized in This Work

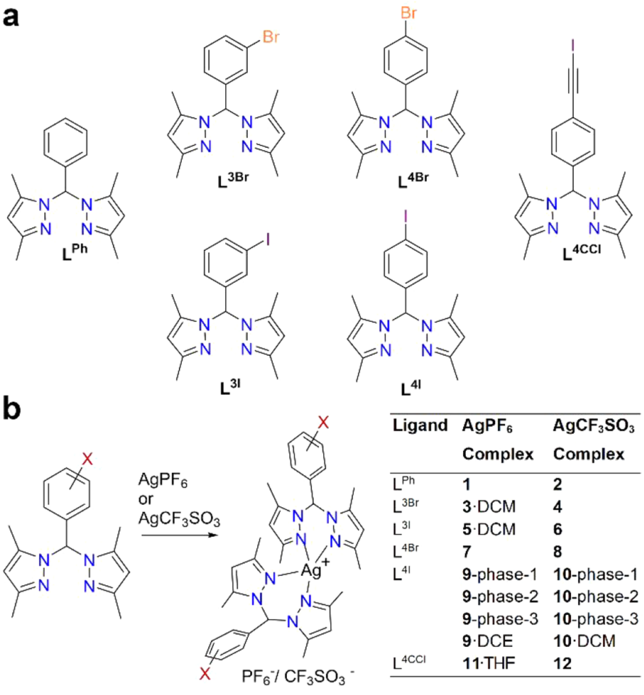

Ligand	$AgPF_6$ Complex	$AgCF_3SO_3$ Complex
L^{Ph}	**1**	**2**
L^{3Br}	**3**·DCM	**4**
L^{3I}	**5**·DCM	**6**
L^{4Br}	**7**	**8**
L^{4I}	**9**-phase-1	**10**-phase-1
	9-phase-2	**10**-phase-2
	9-phase-3	**10**-phase-3
	9·DCE	**10**·DCM
L^{4CCI}	**11**·THF	**12**

phenylbis(pyrazolyl)methane ligand that is devoid of halogen atoms. However, we increase the XB donor potential of these ligands with an alkyno group interposed by an iodine and a phenyl ring. The resulting ligand (L^{4CCI}) is characterized by a large positive charge in the σ-hole, which is potentially capable of forming strong XB interactions.

The complex building units are prepared by reacting the ligands with silver salts ($AgPF_6$ and $AgCF_3SO_3$). Silver usually adopts coordination geometries that vary from linear to tetrahedral.[44−65] Due to the lack of electronic stabilization (d^{10} metal ion), these geometries are usually distorted, and the metal adapts to the steric requirements of the ligands. Thus, two different counteranions are used to provide different systems that can potentially act as halogen bond acceptors (fluorine in PF_6^- or fluorine and oxygen in $CF_3SO_3^-$) as well as having different coordination capabilities toward a metal center. Halogen bonds are present in all the structures obtained with the halogenated ligands, and in two cases, when crystallizing $[Ag(L^{4I})_2]PF_6$ and $[Ag(L^{4I})_2]CF_3SO_3$ in tetrahydrofuran/hexane (THF/Hx), we identify three phases, which differ by their solvent content. Phase-1 is characterized by a honeycomb structure with large 1D channels (diameter of 30 Å), and phase-1 evolves into phase-2 after a spontaneous loss of most of the solvent. Phase-2 presents smaller 1D channels that confine THF molecules, and the evolution from phase-2 to a solventless phase-3 can be promoted by a thermal treatment at 120 °C. The phase-1 to phase-3 transitions are investigated by thermal methods and powder X-ray diffraction. The single-crystal X-ray structures allow the role of the weak interactions in the formation of these supramolecular arrangements to be established. Overall, the analysis of the structural arrangements wishes to provide useful hints for the selection of the appropriate components in the formation of supramolecular systems based on coordination compounds as repetitive units.

■ RESULTS AND DISCUSSION

The Ag^+ complexes are prepared by mixing $AgPF_6$ and $AgCF_3SO_3$ with different ligand (L) systems in a 1/2 ratio. The choice of the two different counteranions is made by considering their different symmetries and potential interactions with metal centers. In particular, the highly symmetric PF_6^- anion exhibits little coordination capability toward Ag^+. In contrast, the $CF_3SO_3^-$ anion has a more pronounced tendency to interact with a metal center, usually as an O-monodentate.[49−52] Both anions, having a net negative charge, can also act as nucleophilic sites for interactions involving positively charged molecular fragments, such as the σ-holes present in halogen atoms or electrophilic CH groups.

The coordination geometries of all of the complexes reported in the present work are depicted in Figures S26−S58. In the structures, the metal appears to be in a distorted tetrahedral environment, but it is difficult to assign a definitive metal geometry to these four-coordinated silver complexes. Hence, it is perhaps useful to employ a τ_4 index that takes into account all the possible distortions from the square-planar to the tetrahedral geometries.[66,67] In all complexes, the τ_4 and τ_4' geometry indices are in the ranges 0.70−0.61 and 0.65−0.46, respectively, which are in line with a seesaw geometry (Table S10). More specifically, two of the four Ag−N coordinative interactions are longer (range 2.34−2.49 Å), and two are shorter (2.21−2.31 Å, Tables S7−S9). As a general observation, in all the reported systems, the metal environment is quite conserved. Hence, we may assume that $[Ag(L)_2]^+$ is a preorganized synthon, with a relatively fixed orientation of phenyl rings attached to a bis-pyrazole moiety. Consequently, the different functionalization of the aromatic ring, with respect to the 3 (meta) and 4 (para) positions, is what dictates the orientations of the halogen atoms (Figure 1). When the halogen atoms are in the 4 position, the conformation of the phenyl ring has little influence on the directionality of the C−X

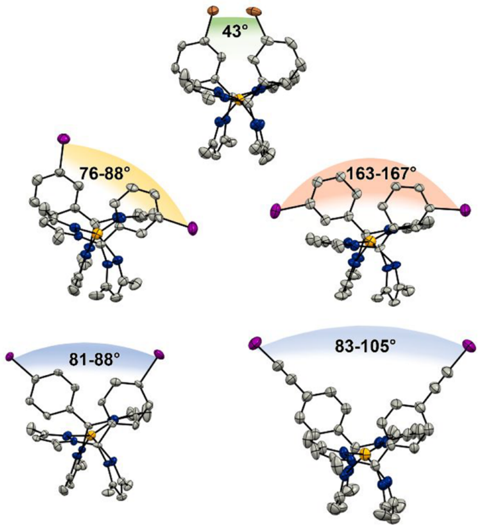

Figure 1. Schematic representation of the multiple experimental orientations, which can be experienced by the halogen atoms after the formation of the Ag complex. The indicated values refer to the observed angles between the C-halogen vector (color codes: C, gray; N, blue; Br, light brown; P, orange; I, purple; Ag, yellow).

vector. In contrast, functionalization of the 3 position leads to different arrangements of the two C−X vectors located on the two ligands. In Figure 2, we report an overview of the intermolecular interaction exchanged between the halogen atoms and the surrounding molecules. More specifically, it can be pointed out how the presence of the halogen atom at position 4 gives rise to two crystal packing motifs involving the anions. In the first one, one halogen atom acts as an XB donor toward the anion, and it simultaneously acts as an XB acceptor toward a second halogen atom (Figure 2h). In the second motif, the anion bridges between two XB donor moieties (Figure 2i,l).[68] The following discussion will focus on the solid-state properties of the silver complexes with the L^{4I} and L^{4CCI} ligands (**9**−**12**; see Scheme 2), which are the systems characterized by preorganized orientations of the two halogen atoms within the $[Ag(L)_2]^+$ moiety. The presence of the alkyne group in L^{4CCI} is devised to increase the XB donor properties of the ligand with respect to L^{4I} while preserving the same spatial orientation of the halogen.[30]

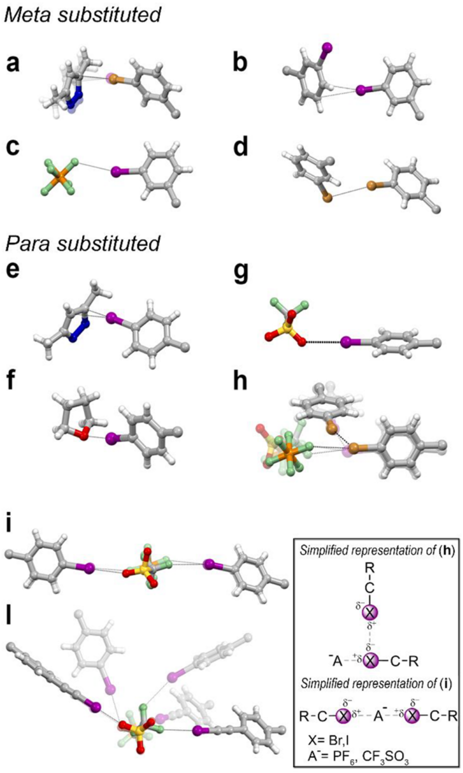

Figure 2. Summary of the XB interactions exchanged by the halogen atoms in the reported structures. The inset describes a simplified representation of XB between two halides and one anion (color codes, C, gray; N, blue; O, red; H, white; F, green; S, yellow; Br, light brown; P, orange; I, purple).

■ SOLVENT ROLE AND PHASE TRANSITIONS

The **9**−**12** complexes are crystallized in different solvent mixtures since it was previously shown that the solvent can have an important role in selecting the type of weak interaction that occurs between two multifunctional molecular counterparts.[69] In our case, the choice of solvent is limited by solubility issues related to the $[Ag(L)_2]^+$/anion complexes, which can dissolve in chlorinated solvents (DCM, DCE) or more polar solvents (acetone, THF, methanol). The crystallizing conditions make use of hexane as an antisolvent. The crystalline material for $[Ag(L^{4I})_2]PF_6$ (**9**) and $[Ag(L^{4I})_2]CF_3SO_3$ (**10**) in the form of different solvates is recovered from the following crystallization conditions: dichloroethane/hexane (DCE/Hx), dichloromethane/hexane (DCM/Hx), and THF/Hx.

More interesting results are obtained from the THF/Hx crystallizing condition, since three different phases can be observed, and the evolution from phase-1 to phase-3 occurs upon decreasing the solvent content. **9**-phase-1 and **10**-phase-1 are characterized by long prismatic crystals (Figure 3 and Figure 4), which are stable in the presence of the mother liquor or when protected by a low temperature environment (less than 200 K). The single-crystal X-ray characterization of these systems shows that they are isostructural, forming large 1D hexagonal cavities filled with solvent molecules (**10**-phase-1 will be described here). When proceeding from the molecular unit to the crystal packing, it can be instructive to analyze the hierarchical construction of the lattice based on the weak XB, CH···F, CH···O, and CH···π interactions. In particular, three molecular units in the inner core are arranged around a PF_6^- or $CF_3SO_3^-$ anion (P18/S18) by means of CH···F or CH···O interactions. Interestingly, toward the periphery of the trimer, the inner iodine atoms of the molecular unit (I6) are directing the σ-hole toward the negative corona of the outermost iodine atom (I3). Even though the halogen−halogen intermolecular distance is particularly long (∼4.5 Å), the geometry of the interaction is preserved, since the C−I6···I3 angle is approximately 160° and close to the theoretical value of 180°. The supramolecular trimers are then piled one over the other by means of CH···F and CH···O interactions mediated by anions bridging different stacking levels along the *c*-axis (Figure 3b). The expansion of the columnar stacking of trimers along the *ab* crystallographic plane is promoted by the anion (P17/S17) that links together two adjacent complex molecules by means of CH···F interactions (Figure 3c). The final supramolecular arrangement results in the formation of a honeycomb structure characterized by hexagonal 1D cavities that are parallel to the crystallographic *c*-axis. Even though the

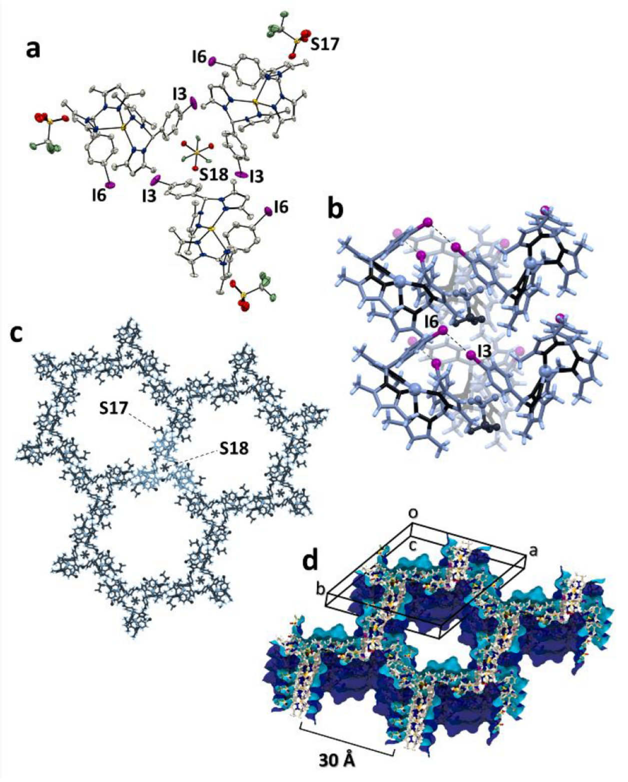

Figure 3. Crystal structure of **10**-phase-1 crystallized in THF/Hx. (a) Supramolecular trimer. (b) Trimeric units piled along the *c*-axis. (c) Expansion of the trimeric unit in the ab crystallographic plane. (d) Crystal packing highlighting the 1D channels.

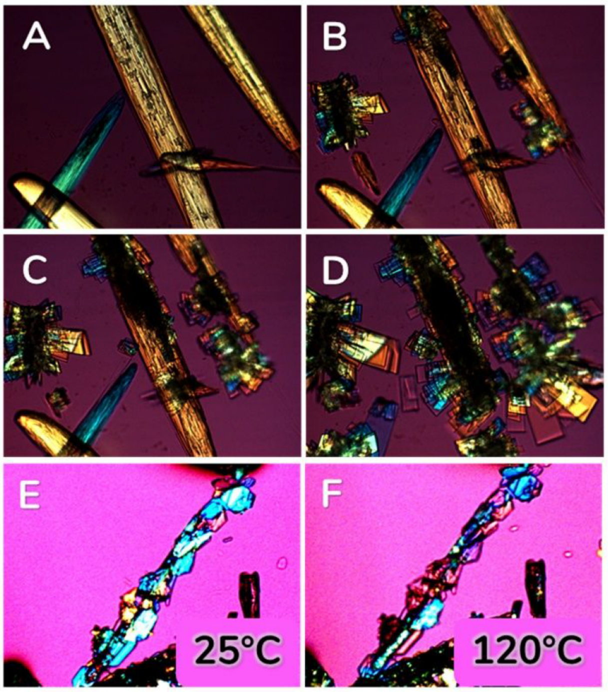

Figure 4. (A)−(D) Polarized microscopy images collected at different points in time showing the phase transition from **10**-phase-1 (needles) to **10**-phase-2 (plates) at RT. (E,F) Hot-stage microscopy images showing the phase transition from 10-phase-2 to **10**-phase-3.

data collection is performed at low temperature, it is possible to identify only some THF molecules in these cavities during crystallization, which are close to the surface of the hexagonal channel. One of these THF molecules exchanges an XB with the I3 atom, which points toward the interior of the cavity (I3···O 1s 3.24 Å, see Figure 2f). It is not possible to identify a reasonable structural model of the solvent into the remaining part of the large 1D cavity, and the Squeeze program is used to determine the residual and diffuse electron density. By taking into account only the complex molecular entity $[Ag(L^{4I})_2]$-CF_3SO_3, which is the building unit of the hexagonal framework, the cavity volume corresponds to 7300 $Å^3$/cell (56% of the unit cell volume), and the 1D cavity diameter is approximately 30 Å (Figure 3d). When the prismatic needle-like crystals of **10**-phase-1 are taken out of the mother liquor, they rapidly change phase and convert into **10**-phase-2 (Figure 4A−D, a video of the single-crystal phase transition is available as a web enhanced object). The time span of the conversion process usually takes significantly less than a minute, and it can be partially hampered by immersing the crystals into viscous matrixes, but the conversion eventually goes to completeness. The **10**-phase-2 crystals exhibit a plate-like morphology, and according to the single-crystal X-ray analysis, they contain one THF molecule per $[Ag(L^{4I})_2]CF_3SO_3$ complex (Figure 5). The complex molecules and the $CF_3SO_3^-$ anions delimit a small channel-like cavity (∼5 Å diameter) hosting the THF molecules. All of the iodine atoms are engaged in XBs with the oxygen or fluorine atoms of the anion, and the I···F interaction distances (3.27 and 3.38 Å) are significantly longer than the I···O interaction distances (2.97 and 2.99 Å). **9**-phase-2 is isomorphous with **10**-phase-2, as reported in the Supporting Information (Table S1 and Figure S44). **10**-phase-2 is stable for several weeks at room temperature; however, when the plate-like crystals are heated above 130 °C, they convert into **10**-phase-3, as reported in Figure 4E,F (a video of the SC to SC phase transition is available as a web enhanced object). After the thermal treatment, the crystals were partially fractured, but a small sample could be used for the single-crystal X-ray data collection (see Figure 5f). The structural analysis revealed that the system has experienced a significant spatial reorganization resulting in a more compact structure with negligible residual voids; hence, **10**-phase-3 can be considered the completely desolvated phase. Only I3 exchanges an XB with an oxygen atom of the anion (3.14 Å; see Figure 2g), whereas the second iodine atom I6 interacts with a methyl group by virtue of its negatively charged corona surrounding the σ-hole. Interestingly, **10**-phase-3 exhibits a different structural organization than **9**-phase-3. The latter phase is also closely packed and forms without a solvent. Nevertheless, in this case, both iodine atoms act as XB donors, in line with one of the structural motifs involving the halogen atoms reported in Figure 2h. In fact, I3 simultaneously acts as an XB donor (toward the anion, I6···F17, 3.221 Å) and an acceptor (toward I6, I3···I6, 3.646 Å). **9**-phase-3 can be obtained after a thermal treatment at 130 °C of **9**-phase-2, but interestingly, it can also be obtained by direct crystallization from a DCM/Hx mixture (Figure 6).

■ POWDER X-RAY DIFFRACTION

Powder X-ray diffraction is performed for compounds **9** and **10** to confirm the phase composition in the bulk and to monitor the conversion between the three phases. For both compounds, phase-1 is the most difficult to characterize

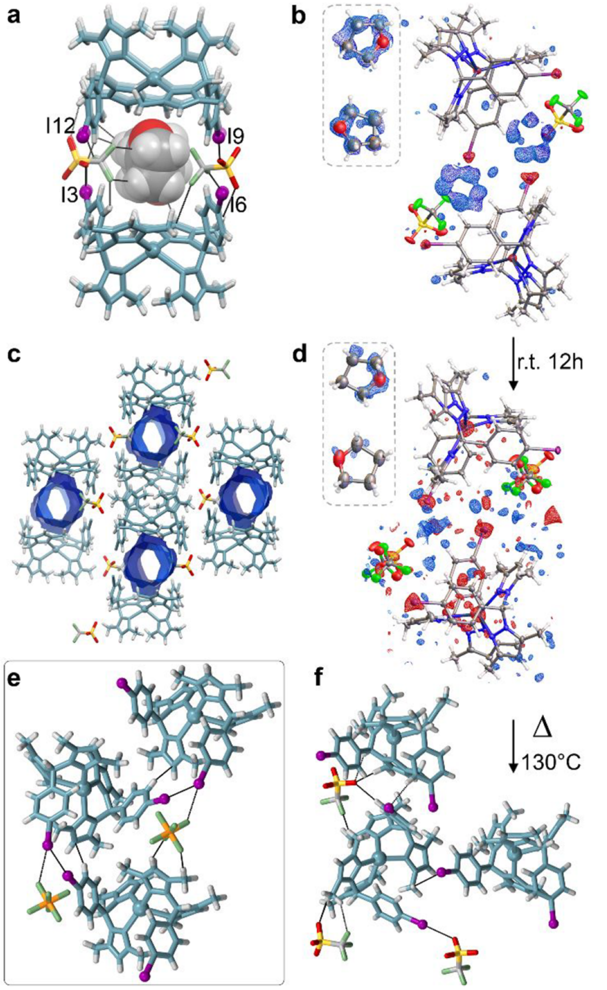

Figure 5. Views of the intermolecular interactions (a) and crystal packing (c) for **10**-phase-2 (THF molecules in a space-filling model). Single-crystal to single-crystal phase transition from **10**-phase-2 to **10**-phase-3 due to the loss of solvent and thermal treatment (b, d, f). Representation of the interactions (dashed bonds) exchanged by the anions and the complex molecules for **9**-phase-3 (e). The insets in (b) and (d) describe the decrease in the residual electron density associated with the THF molecules.

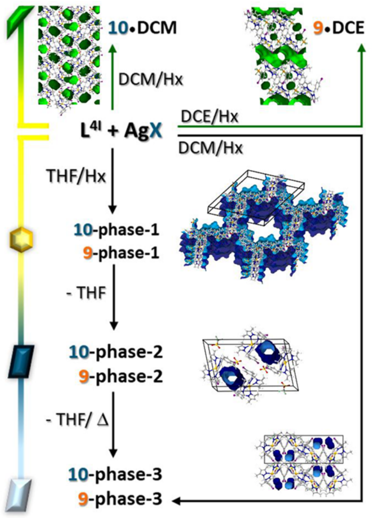

Figure 6. Schematic representation of the phase transitions and the solvates of **9** and **10** described in this work.

experimentally since the long prismatic crystals are very unstable once removed from the mother liquor (THF/Hx). Wet crystals are placed onto the sample holder and covered with a protective film as described in the experimental section (General Methods in Supporting Information). The crystals are not ground to prevent phase transformations; hence, the data collection is affected by significant preferential orientation. Figure 7 shows the comparison between the experimental PXRD of **10**-phase-1 with the calculated patterns derived by SC-XRD.[70] There is good agreement between the predicted and experimental diffractograms, which is particularly true for the peak positions, while the relative intensities are affected by the cited strong preferential orientation and sample roughness. The conversion of phase-1 into phase-2 is very fast, and it went to completion in approximately 30 s after the removal of the film and the evaporation of the solvent. The rapid evolution from phase-1 to phase-2 implies that the investigation based on the thermal analysis (DSC and TGA; see below) exclusively involves phase-2 even when starting from the long prismatic crystals of phase-1. The plate-like crystals of phase-2 are stable for several days; however, it is interesting to note that the solvent content of phase-2 is not constant over time. In fact, the SC-XRD data collection of a freshly mounted crystal shows one THF molecule per complex molecular entity, whereas after the crystal is left for 24 h at room temperature and in the absence of the crystallizing solvent, the solvent content decreases to 0.25 per complex molecule (compare Figure 5b,d). This observation is in line with the presence of the narrow channels that characterize phase-2 and that contain the THF molecules, which weakly interact with complex cations and anions. The relatively small size of the channels implies that the removal of the solvent can be tolerated without the system undergoing structural reorganization. Phase-2 of the two compounds is isostructural, but after the thermal treatment, they give rise to two different phase-3's (Figures 7g and S21).

■ THERMAL ANALYSIS

As pointed out in the PXRD section, the transformation from hexagonal phase-1 to phase-2 for both systems is very rapid once they are removed from the mother liquor (THF/Hx), and it occurs in a time span of a few seconds. Hence, the thermal experiments monitor the events occurring between phase-2 and phase-3. The hexagonal prims of **10**-phase-1 are dried prior to performing the experiments to remove the solvent wetting the crystals. The DSC profile shows the presence of an exothermic peak at 113 °C with a shoulder at the beginning of the event (Figure 7B). The exothermic peak is associated with the phase-2 to phase-3 conversion, whereas a minor endothermic event can be associated with the residual THF desorption within the channels of **10**-phase-2. There are no other events occurring when decreasing the temperature to room temperature (RT) and then increasing the temperature above 200 °C. The TGA profile of **10**-phase-2 shows no appreciable weight loss at approximately 120 °C, but the compound undergoes decomposition at 221 °C.

For **9**, we grew plate-like crystals corresponding to **9**-phase-2, which were then used for the thermal experiments (Figure S17). In the DSC scan, there is an endothermic peak at 111 °C associated with the loss of the solvent into the small channels, and concomitantly, the systems experience a structural

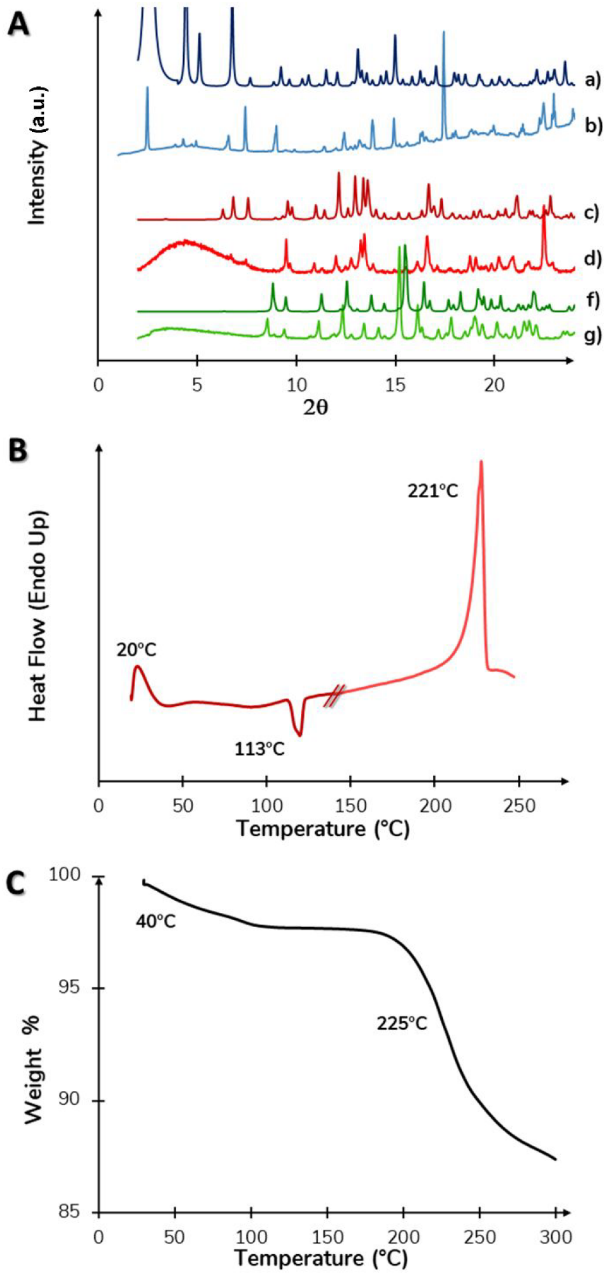

Figure 7. (A) Overlap between the simulated and experimental PXRD of **10**: 10-phase-1 (a,b), **10**-phase-2 (c,d), **10**-phase-3 (f,g). (B) DSC and (C) TGA traces for **10**-phase-2.

reorganization to the more stable **9**-phase-3. There are no other events taking place when decreasing the temperature to RT and then increasing the temperature above 200 °C. At 264 °C, the system undergoes decomposition. The loss of solvent at 111 °C is confirmed by a 5% weight loss, in agreement with 1 molecule of THF per $[Ag(L^{4I})_2]PF_6$ (6% theoretical), Figure S18.

A LONGER SYNTHON: $[Ag(L^{4CCI})_2]^+$

As pointed out earlier in the discussion, the presence of an iodoalkyne functional group confers to the ligand a greater propensity to act as an XB donor with respect to the L^{4I} ligand, with L^{4CCI} having a more pronounced σ-hole and negative corona on the halogen atom. The molecular structures of $[Ag(L^{4CCI})_2](PF_6)$·THF (**11**·THF) and $[Ag(L^{4CCI})_2]$-(CF_3SO_3) (**12**) are reported in Figure 8. In both compounds, the anions bridge two complex cations by means of an XB with the peripheral iodine atoms, in agreement with the second motif described above for the XB reported in this work (see Figure 2l). In particular, in **12**, $CF_3SO_3^-$ acts as an XB acceptor toward two opposite iodine atoms (I3···O1T, 2.844 Å; I6···F2TB, 3.059 Å); in **11**·THF, PF_6^- engages two cis-fluorine atoms into an XB formation with symmetry-related iodine atoms (I3···F24B, 2.987 Å; I3···F24A, 2.960 Å). The result is the formation of supramolecular chains in both cases, even though they each express a different structural packing. In fact, in **12**, the chains are more interwoven, leaving no residual void for the presence of solvent during crystallization. In contrast, in **11**·THF, the chains delimit channel-like cavities filled with disordered THF molecules during crystallization. Obviously, in **11**·THF and **12**, the presence of the Ph—C≡C—I group with respect to the Ph—I moiety in **9** increases the dimension of the supramolecular synthon, which is represented by the $[Ag(L)_2]^+$ complex cation. However, by comparing the structures of **11**·THF, **12**, and **9**/**10**-phase-1, it is evident that increasing the length of the XB donor moiety does not produce systems characterized by large channels as in the **9**/**10**-phase-1.

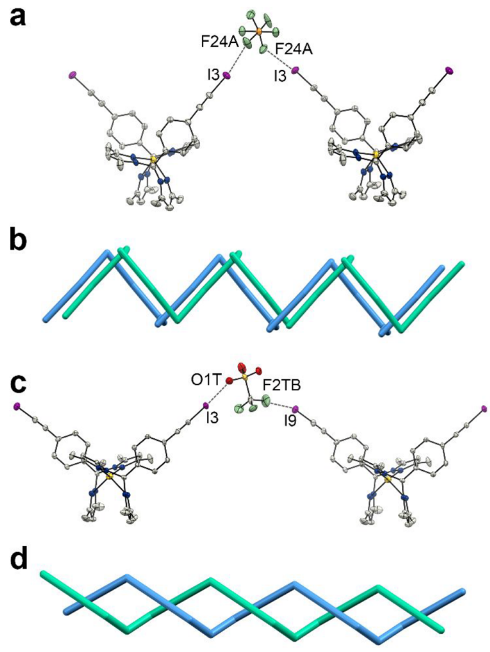

Figure 8. Halogen bond interactions for **11**·THF (a) and **12** (c). Schematic representations of the supramolecular chains in **11**·THF (b) and **12** (d).

CONCLUSIONS

The ligands described here are characterized by two functions, one that can bind a metal center (N,N system) and the other that can form directional supramolecular interactions (halogen atoms). The assemblies generated with Ag^+ result in an almost invariant molecular geometry, with the cation in a well-defined, even though distorted, tetrahedral environment. The reason for such behavior can be ascribed to the presence of the moderate steric hindrance provided by the methyl groups attached to the pyrazole rings. Consequently, when the two ligands are bound to the metal center, they are interlocked to minimize steric repulsion. The result is a preorganized XB donor directionality, which exclusively depends on the position of the halogen functionalization on the phenyl ring. When comparing all of the reported structures, it appears that with L^{4X} and L^{4CCI}, there are two repetitive structural motifs. The first one is $X^{\delta+}\cdots{}^{-\delta}X^{\delta+}\cdots$Anion, with the central halogen atoms acting simultaneously as XB donors and acceptors, and the second corresponds to $X^{\delta+}\cdots$Anion$\cdots{}^{+\delta}X$, with the anion forming a bridge between the two XB donors (see Figure 2).

The $[Ag(L^{4I})_2]PF_6/CF_3SO_3$ systems crystallized from THF/Hx are characterized by the presence of three phases. The conversion from phase-1 to phase-3 occurs by a stepwise decrease in the solvent content and by a reinforcement of the XB interactions among the molecular components. **9**/**10**-phase-1 presents a supramolecular structure with a large columnar cavity filled with solvent molecules, and we have not investigated the various methodologies that are suitable to activate porous materials that are characterized by large cavities occupied with solvent−guest molecules. These methods are usually applied to metal organic frameworks,[71] in which the weakest type of interaction is the metal−ligand coordination bond, which is significantly stronger than the XB or other weak interactions found in the reported structures.

Even though the Ph—Br and Ph—I moieties may be considered moderately good XB donors, the XB donor potential of these ligands can be increased by introducing additional electron withdrawing groups on the aromatic fragment, hence increasing the positive charge of the σ-hole.[30] L^{4CCI} was therefore devised to increase the strength of the XB interactions. A summary of the normalized distances[72−74] pertaining to the XBs described here is provided in Figure 9. Generally, it is clear that shorter interactions are experienced with the oxygen atom of the $CF_3SO_3^-$ anion and iodine compared to those of the other interactions. This observation is also in agreement with the propensity of $CF_3SO_3^-$ to act as an O-monodentate ligand toward a metal center when compared to PF_6^-. It is also evident that there is a significant decrease in the XB distance along the Br < I < C≡C—I series. This observation is consistent with a more pronounced σ-hole on L^{4CCI} with respect to L^{4I}. As a result, more robust interactions can potentially be formed with this ligand, and the high directionality of the XB allows for significant control over the supramolecular arrangements. The studied systems provide insight into the choice of molecular components for the construction of supramolecular assemblies comprising coordination entities as building units.

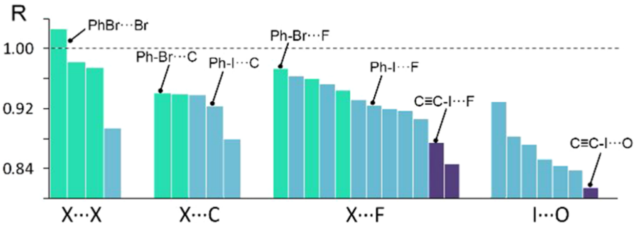

Figure 9. Plot of the normalized distance R for the XB interactions. A value of 1 corresponds to an XB donor−acceptor distance equal to the sum of the v.d.W. radii.

■ ASSOCIATED CONTENT

Supporting Information

The Supporting Information is available free of charge at https://pubs.acs.org/doi/10.1021/acs.inorgchem.0c00256.

> Synthesis of the ligands and complexes, NMR spectra, single-crystal structures, optical microscope images, crystallographic tables, geometric parameters, τ_4 indices, thermal analyses (DSC and TGA), and powder X-ray diffraction spectra (PDF)

Web-Enhanced Features

Single-crystal to single-crystal phase transitions **10**-phase-1/**10**-phase-2/**10**-phase-3 in an MPEG format are available in the HTML version of the paper.

Accession Codes

CCDC 1902455−1902465 and 1968843−1968848 contain the supplementary crystallographic data for this paper. These data can be obtained free of charge via www.ccdc.cam.ac.uk/data_request/cif, or by emailing data_request@ccdc.cam.ac.uk, or by contacting The Cambridge Crystallographic Data Centre, 12 Union Road, Cambridge CB2 1EZ, UK; fax: +44 1223 336033.

■ AUTHOR INFORMATION

Corresponding Author

Luciano Marchiò − *Dipartimento di Scienze Chimiche, della Vita e della Sostenibilità Ambientale (Chemistry Unit), Università di Parma 43124 Parma, Italy*; orcid.org/0000-0002-0025-1104; Email: luciano.marchio@unipr.it

Authors

Giulia Bonfant − *Dipartimento di Scienze Chimiche, della Vita e della Sostenibilità Ambientale (Chemistry Unit), Università di Parma 43124 Parma, Italy*; orcid.org/0000-0001-5108-8354

Matteo Melegari − *Dipartimento di Scienze Chimiche, della Vita e della Sostenibilità Ambientale (Chemistry Unit), Università di Parma 43124 Parma, Italy*

Davide Balestri − *Dipartimento di Scienze Chimiche, della Vita e della Sostenibilità Ambientale (Chemistry Unit), Università di Parma 43124 Parma, Italy*; orcid.org/0000-0003-3493-9115

Francesco Mezzadri − *Dipartimento di Scienze Chimiche, della Vita e della Sostenibilità Ambientale (Chemistry Unit), Università di Parma 43124 Parma, Italy*; orcid.org/0000-0001-9505-1457

Vittoria Marzaroli − *Dipartimento di Scienze Chimiche, della Vita e della Sostenibilità Ambientale (Chemistry Unit), Università di Parma 43124 Parma, Italy*; orcid.org/0000-0003-1781-2622

Irene Bassanetti − *Dipartimento di Scienze Chimiche, della Vita e della Sostenibilità Ambientale (Chemistry Unit), Università di Parma 43124 Parma, Italy*; orcid.org/0000-0003-0618-5440

Complete contact information is available at: https://pubs.acs.org/10.1021/acs.inorgchem.0c00256

Notes

The authors declare no competing financial interest.

■ ACKNOWLEDGMENTS

This work benefited from the equipment and framework of the COMP-HUB Initiative, funded by the “Departments of Excellence” program of the Italian Ministry for Education, University and Research (MIUR, 2018-2022). Chiesi Farmaceutici SpA is acknowledged for the support of the D8 Venture X-ray equipment. The COST action CM1402 “Crystallize” is acknowledged for networking support.

■ REFERENCES

(1) Leong, W. L.; Vittal, J. J. One-Dimensional Coordination Polymers: Complexity and Diversity in Structures, Properties, and Applications. *Chem. Rev.* **2011**, *111*, 688−764.

(2) Cook, T. R.; Zheng, Y.-R.; Stang, P. J. Metal−Organic Frameworks and Self-Assembled Supramolecular Coordination Complexes: Comparing and Contrasting the Design, Synthesis, and Functionality of Metal−Organic Materials. *Chem. Rev.* **2013**, *113*, 734−777.

(3) Kitagawa, S.; Kitaura, R.; Noro, S. Functional Porous Coordination Polymers. *Angew. Chem., Int. Ed.* **2004**, *43*, 2334−2375.

(4) Janiak, C. Engineering Coordination Polymers towards Applications. *Dalton Trans.* **2003**, No. 14, 2781−2804.

(5) Ahmed, F.; Roy, S.; Naskar, K.; Sinha, C.; Alam, S. M.; Kundu, S.; Vittal, J. J.; Mir, M. H. Halogen···Halogen Interactions in the Supramolecular Assembly of 2D Coordination Polymers and the CO_2 Sorption Behavior. *Cryst. Growth Des.* **2016**, *16*, 5514−5519.

(6) Roy, S.; Titi, H. M.; Tripuramallu, B. K.; Bhunia, N.; Verma, R.; Goldberg, I. Silver Coordination Polymers Based on Newly Designed Bis(Cyanobenzyl)Bipiperidine Ligand: Synthesis, Anion Exchange, Guest Inclusion, Electrochemical, and Photoluminescence Properties. *Cryst. Growth Des.* **2016**, *16*, 2814−2825.

(7) Zhang, J.; Wang, C.-C.; Wang, P.; Cao, Y.-L. Selective Uptake of Organic Dyes in a Silver-Based Coordination Polymer. *RSC Adv.* **2016**, *6*, 73595−73599.

(8) Haldar, R.; Matsuda, R.; Kitagawa, S.; George, S. J.; Maji, T. K. Amine-Responsive Adaptable Nanospaces: Fluorescent Porous Coordination Polymer for Molecular Recognition. *Angew. Chem., Int. Ed.* **2014**, *53*, 11772−11777.

(9) Kan, W.-Q.; Ma, J.-F.; Liu, Y.-Y.; Yang, J. A Series of Coordination Polymers Based on 5-(2-Carboxybenzyloxy) Isophthalic Acid and Bis(Imidazole) Ligands: Syntheses, Topological Structures and Photoluminescent Properties. *CrystEngComm* **2012**, *14*, 2316−2326.

(10) Journaux, Y.; Ferrando-Soria, J.; Pardo, E.; Ruiz-Garcia, R.; Julve, M.; Lloret, F.; Cano, J.; Li, Y.; Lisnard, L.; Yu, P.; Stumpt, H.; Pereira, C. L. M. Design of Magnetic Coordination Polymers Built from Polyoxalamide Ligands: A Thirty Year Story. *Eur. J. Inorg. Chem.* **2018**, *2018*, 228−247.

(11) López-Cabrelles, J.; Mañas-Valero, S.; Vitórica-Yrezábal, I. J.; Bereciartua, P. J.; Rodríguez-Velamazán, J. A.; Waerenborgh, J. C.; Vieira, B. J. C.; Davidovikj, D.; Steeneken, P. G.; Van der Zant, H. S. J.; Mìnguez Espallargas, G.; Coronado, E. Isoreticular Two-Dimensional Magnetic Coordination Polymers Prepared through Pre-Synthetic Ligand Functionalization. *Nat. Chem.* **2018**, *10*, 1001−1007.

(12) Georgiev, I. G.; MacGillivray, L. R. Metal-Mediated Reactivity in the Organic Solid State: From Self-Assembled Complexes to Metal−Organic Frameworks. *Chem. Soc. Rev.* **2007**, *36*, 1239−1247.

(13) Libri, S.; Mahler, M.; Mínguez Espallargas, G.; Singh, D. C. N. G.; Soleimannejad, J.; Adams, H.; Burgard, M. D.; Rath, N. P.; Brunelli, M.; Brammer, L. Ligand Substitution within Nonporous Crystals of a Coordination Polymer: Elimination from and Insertion into Ag-O Bonds by Alcohol Molecules in a Solid−Vapor Reaction. *Angew. Chem., Int. Ed.* **2008**, *47*, 1693−1697.

(14) Kole, G. K.; Tan, G. K.; Vittal, J. J. Photoreactivity of Ag(I) Complexes and Coordination Polymers of Pyridyl Acrylic Acids. *Cryst. Growth Des.* **2012**, *12*, 326−332.

(15) Chu, Q.; Swenson, D. C.; MacGillivray, L. R. A Single-Crystal-to-Single-Crystal Transformation Mediated by Argentophilic Forces Converts a Finite Metal Complex into an Infinite Coordination Network. *Angew. Chem., Int. Ed.* **2005**, *44*, 3569−3572.

(16) Park, I.-H.; Lee, E.; Lee, S. S.; Vittal, J. J. Chemical Patterning in Single Crystals of Metal-Organic Frameworks by [2 + 2] Cycloaddition Reaction. *Angew. Chem., Int. Ed.* **2019**, *58*, 14860−14864.

(17) Desiraju, G. R.; Vittal, J. J.; Ramanan, A. *Crystal Engineering - A Textbook*; Co-Published with Indian Institute of Science (IISc): Bangalore, India, 2011.

(18) Xu, L.; Shen, X.; Zhou, Z.; He, T.; Zhang, J.; Qiu, H.; Saha, M. L.; Yin, S.; Stang, P. J. Metallacycle-Cored Supramolecular Polymers: Fluorescence Tuning by Variation of Substituents. *J. Am. Chem. Soc.* **2018**, *140*, 16920−16924.

(19) Braga, D.; Desiraju, G. R.; Miller, J. S.; Orpen, A. G.; Price, S. (Sally) L. Innovation in Crystal Engineering. *CrystEngComm* **2002**, *4*, 500−509.

(20) Maly, K. E.; Gagnon, E.; Maris, T.; Wuest, J. D. Engineering Hydrogen-Bonded Molecular Crystals Built from Derivatives of Hexaphenylbenzene and Related Compounds. *J. Am. Chem. Soc.* **2007**, *129*, 4306−4322.

(21) Li, P.; He, Y.; Guang, J.; Weng, L.; Zhao, J. C.-G.; Xiang, S.; Chen, B. A Homochiral Microporous Hydrogen-Bonded Organic Framework for Highly Enantioselective Separation of Secondary Alcohols. *J. Am. Chem. Soc.* **2014**, *136*, 547−549.

(22) Metrangolo, P.; Resnati, G. Halogen Bonding: A Paradigm in Supramolecular Chemistry. *Chem. - Eur. J.* **2001**, *7*, 2511−2519.

(23) Cavallo, G.; Metrangolo, P.; Milani, R.; Pilati, T.; Priimagi, A.; Resnati, G.; Terraneo, G. The Halogen Bond. *Chem. Rev.* **2016**, *116*, 2478−2601.

(24) Hunter, C. A.; Sanders, J. K. M. The Nature of π-π Interactions. *J. Am. Chem. Soc.* **1990**, *112*, 5525−5534.

(25) Sinnokrot, M. O.; Valeev, E. F.; Sherrill, C. D. Estimates of the Ab Initio Limit for π-π Interactions: The Benzene Dimer. *J. Am. Chem. Soc.* **2002**, *124*, 10887−10893.

(26) Beatty, A. M. Open-Framework Coordination Complexes from Hydrogen-Bonded Networks: Toward Host/Guest Complexes. *Coord. Chem. Rev.* **2003**, *246*, 131−143.

(27) Bassanetti, I.; Bracco, S.; Comotti, A.; Negroni, M.; Bezuidenhout, C.; Canossa, S.; Mazzeo, P. P.; Marchió, L.; Sozzani, P. Flexible Porous Molecular Materials Responsive to CO_2, CH_4 and Xe Stimuli. *J. Mater. Chem. A* **2018**, *6*, 14231−14239.

(28) Lapadula, G.; Judaš, N.; Friščić, T.; Jones, W. A Three-Component Modular Strategy to Extend and Link Coordination Complexes by Using Halogen Bonds to O, S and π Acceptors. *Chem. - Eur. J.* **2010**, *16*, 7400−7403.

(29) Desiraju, G. R.; Ho, P. S.; Kloo, L.; Legon, A. C.; Marquardt, R.; Metrangolo, P.; Politzer, P.; Resnati, G.; Rissanen, K. Definition of the Halogen Bond (IUPAC Recommendations 2013). *Pure Appl. Chem.* **2013**, *85*, 1711−1713.

(30) Aakeröy, C. B.; Wijethunga, T. K.; Desper, J.; Daković, M. Crystal Engineering with Iodoethynylnitrobenzenes: A Group of Highly Effective Halogen-Bond Donors. *Cryst. Growth Des.* **2015**, *15*, 3853−3861.

(31) Turunen, L.; Pan, F.; Beyeh, N. K.; Cetina, M.; Trant, J. F.; Ras, R. H. A.; Rissanen, K. Halogen-Bonded Solvates of Tetrahaloethynyl Cavitands. *CrystEngComm* **2017**, *19*, 5223−5229.

(32) Ormond-Prout, J. E.; Smart, P.; Brammer, L. Cyanometallates as Halogen Bond Acceptors. *Cryst. Growth Des.* **2012**, *12*, 205−216.

(33) Awwadi, F. F.; Taher, D.; Haddad, S. F.; Turnbull, M. M. Competition between Hydrogen and Halogen Bonding Interactions: Theoretical and Crystallographic Studies. *Cryst. Growth Des.* **2014**, *14*, 1961−1971.

(34) Ivanov, D. M.; Novikov, A. S.; Ananyev, I. V.; Kirina, Y. V.; Kukushkin, V. Y. Halogen Bonding between Metal Centers and Halocarbons. *Chem. Commun.* **2016**, *52*, 5565−5568.

(35) Sattler, W.; Ruccolo, S.; Parkin, G. Synthesis, Structure, and Reactivity of a Terminal Organozinc Fluoride Compound: Hydrogen Bonding, Halogen Bonding, and Donor−Acceptor Interactions. *J. Am. Chem. Soc.* **2013**, *135*, 18714−18717.

https://dx.doi.org/10.1021/acs.inorgchem.0c00256
Inorg. Chem. XXXX, XXX, XXX−XXX

(36) Politzer, P.; Murray, J. S.; Clark, T. Halogen Bonding: An Electrostatically-Driven Highly Directional Noncovalent Interaction. *Phys. Chem. Chem. Phys.* **2010**, *12*, 7748−7757.

(37) Clark, T.; Hennemann, M.; Murray, J. S.; Politzer, P. Halogen Bonding: The σ-Hole. *J. Mol. Model.* **2007**, *13*, 291−296.

(38) Li, B.; Zang, S.-Q.; Wang, L.-Y.; Mak, T. C. W. Halogen Bonding: A Powerful, Emerging Tool for Constructing High-Dimensional Metal-Containing Supramolecular Networks. *Coord. Chem. Rev.* **2016**, *308*, 1−21.

(39) Brammer, L.; Mínguez Espallargas, G.; Libri, S. Combining Metals with Halogen Bonds. *CrystEngComm* **2008**, *10*, 1712−1727.

(40) Johnson, M. T.; Džolić, Z.; Cetina, M.; Wendt, O. F.; Öhrström, L.; Rissanen, K. Neutral Organometallic Halogen Bond Acceptors: Halogen Bonding in Complexes of PCPPdX (X = Cl, Br, I) with Iodine (I_2), 1,4-Diiodotetrafluorobenzene (F4DIBz), and 1,4-Diiodooctafluorobutane (F8DIBu). *Cryst. Growth Des.* **2012**, *12*, 362−368.

(41) Clemente-Juan, J. M.; Coronado, E.; Mínguez Espallargas, G.; Adams, H.; Brammer, L. Effects of Halogen Bonding in Ferromagnetic Chains Based on Co(II) Coordination Polymers. *CrystEngComm* **2010**, *12*, 2339−2342.

(42) Atzori, M.; Artizzu, F.; Sessini, E.; Marchiò, L.; Loche, D.; Serpe, A.; Deplano, P.; Concas, G.; Pop, F.; Avarvari, N.; Laura Mercuri, M. Halogen-Bonding in a New Family of Tris(Haloanilato)-Metallate(III) Magnetic Molecular Building Blocks. *Dalton Trans.* **2014**, *43*, 7006−7019.

(43) Thangavadivale, V.; Aguiar, P. M.; Jasim, N. A.; Pike, S. J.; Smith, D. A.; Whitwood, A. C.; Brammer, L.; Perutz, R. N. Self-Complementary Nickel Halides Enable Multifaceted Comparisons of Intermolecular Halogen Bonds: Fluoride Ligands vs. Other Halides. *Chem. Sci.* **2018**, *9*, 3767−3781.

(44) Almotawa, R. M.; Aljomaih, G.; Trujillo, D. V.; Nesterov, V. N.; Rawashdeh-Omary, M. A. New Coordination Polymers of Copper(I) and Silver(I) with Pyrazine and Piperazine: A Step Toward "Green" Chemistry and Optoelectronic Applications. *Inorg. Chem.* **2018**, *57*, 9962−9976.

(45) Wu, H.-P.; Janiak, C.; Rheinwald, G.; Lang, H. 5,5′-Dicyano-2,2′-Bipyridine Silver Complexes: Discrete Units or Co-Ordination Polymers through a Chelating and/or Bridging Metal−Ligand Interaction. *J. Chem. Soc., Dalton Trans.* **1999**, *0*, 183−190.

(46) Genuis, E. D.; Kelly, J. A.; Patel, M.; McDonald, R.; Ferguson, M. J.; Greidanus-Strom, G. Coordination Polymers from the Self-Assembly of Silver(I) Salts and Two Nonlinear Aliphatic Dinitrile Ligands, Cis −1,3-Cyclopentanedicarbonitrile and Cis −1,3-Bis-(Cyanomethyl)Cyclopentane: Synthesis, Structures, and Photoluminescent Properties. *Inorg. Chem.* **2008**, *47*, 6184−6194.

(47) Ma, Z.; Shi, H.; Deng, X.; Guedes da Silva, M. F. C.; Martins, L. M. D. R. S.; Pombeiro, A. J. L. Silver Coordination Polymers with Tri- and Hexacyanoethyl-Functionalized Macrocyclic Ligands. *Dalton Trans.* **2015**, *44*, 1388−1396.

(48) Bassanetti, I.; Marchiò, L. Structural Variability in Ag(I) and Cu(I) Coordination Polymers with Thioether-Functionalized Bis-(Pyrazolyl)Methane Ligands. *Inorg. Chem.* **2011**, *50*, 10786−10797.

(49) Bassanetti, I.; Atzeri, C.; Tinonin, D. A.; Marchiò, L. Silver(I) and Thioether-Bis(Pyrazolyl)Methane Ligands: The Correlation between Ligand Functionalization and Coordination Polymer Architecture. *Cryst. Growth Des.* **2016**, *16*, 3543−3552.

(50) Bassanetti, I.; Mezzadri, F.; Comotti, A.; Sozzani, P.; Gennari, M.; Calestani, G.; Marchiò, L. Influence of Anions in Silver Supramolecular Frameworks: Structural Characteristics and Sorption Properties. *J. Am. Chem. Soc.* **2012**, *134*, 9142−9145.

(51) Bassanetti, I.; Comotti, A.; Sozzani, P.; Bracco, S.; Calestani, G.; Mezzadri, F.; Marchiò, L. Porous Molecular Crystals by Macrocyclic Coordination Supramolecules. *J. Am. Chem. Soc.* **2014**, *136*, 14883−14895.

(52) Gardinier, J. R.; Tatlock, H. M.; Hewage, J. S.; Lindeman, S. V. Cyclic versus Polymeric Supramolecular Architectures in Metal Complexes of Dinucleating Ligands: Silver(I) Trifluoromethanesulfonate Complexes of the Isomers of Bis(Di(1H-Pyrazolyl)Methyl)-1,1′-Biphenyl. *Cryst. Growth Des.* **2013**, *13*, 3864−3877.

(53) Morin, T. J.; Merkel, A.; Lindeman, S. V.; Gardinier, J. R. Breaking the Cycle: Impact of Sterically-Tailored Tetra(Pyrazolyl)-Lutidines on the Self-Assembly of Silver(I) Complexes. *Inorg. Chem.* **2010**, *49*, 7992−8002.

(54) Muñoz-Molina, J. M.; Belderrain, T. R.; Pérez, P. J. Group 11 Tris(Pyrazolyl)Methane Complexes: Structural Features and Catalytic Applications. *Dalton Trans.* **2019**, *48*, 10772−10781.

(55) Almeida, J.; Roma-Rodrigues, C.; Mahmoud, A. G.; Guedes da Silva, M. F. C.; Pombeiro, A. J. L.; Martins, L. M. D. R. S.; Baptista, P. V.; Fernandes, A. R. Structural Characterization and Biological Properties of Silver(I) Tris(Pyrazolyl)Methane Sulfonate. *J. Inorg. Biochem.* **2019**, *199*, 110789−110790.

(56) Durá, G.; Carrión, M. C.; Jalón, F. A.; Rodríguez, A. M.; Manzano, B. R. Metal Supramolecular Frameworks with Silver and Ditopic Bis(Pyrazolyl)Methane Ligands: Effect of the Anions and Ligand Substitution. *Cryst. Growth Des.* **2014**, *14*, 3510−3529.

(57) Durá, G.; Carrión, M. C.; Jalón, F. A.; Rodríguez, A. M.; Manzano, B. R. Self-Assembly of Silver(I) and Ditopic Heteroscorpionate Ligands. Spontaneous Chiral Resolution in Helices and Sequence Isomerism in Coordination Polymers. *Cryst. Growth Des.* **2013**, *13*, 3275−3282.

(58) Durá, G.; Carrión, M. C.; Jalón, F. A.; Manzano, B. R.; Rodríguez, A. M.; Mereiter, K. Robust 2D Coordination Networks from a Two-Step Assembly Process with Predesigned Silver Cyclic Dimers and Hexamethylenetetramine. *Cryst. Growth Des.* **2015**, *15*, 3321−3331.

(59) Manzano, B. R.; Jalón, F. A.; Carrión, M. C.; Durá, G. Bis(Pyrazol-1-Yl)(Pyridin-x-Yl)Methane Ligands - Mono- or Ditopic Ligands in Complexes and Supramolecular Frameworks. *Eur. J. Inorg. Chem.* **2016**, *2016*, 2272−2295.

(60) Pettinari, C.; Marchetti, F.; Orbisaglia, S.; Pettinari, R.; Ngoune, J.; Gómez, M.; Santos, C.; Álvarez, E. Group 11 Complexes with the Bidentate Di(1H-Indazol-1-Yl)Methane and Di(2H-Indazol-2-Yl)Methane) Ligands. *CrystEngComm* **2013**, *15*, 3892−3907.

(61) Pettinari, C.; Tăbăcaru, A.; Galli, S. Coordination Polymers and Metal−Organic Frameworks Based on Poly(Pyrazole)-Containing Ligands. *Coord. Chem. Rev.* **2016**, *307*, 1−31.

(62) Reger, D. L.; Brown, K. J.; Gardinier, J. R.; Smith, M. D. Synthesis and Structural Characterization of a Bitopic Ferrocenyl-Linked Bis(Pyrazolyl)Methane Ligand and Its Silver(I) Coordination Polymers. *Organometallics* **2003**, *22*, 4973−4983.

(63) Reger, D. L.; Watson, R. P.; Gardinier, J. R.; Smith, M. D. Impact of Variations in Design of Flexible Bitopic Bis(Pyrazolyl)-Methane Ligands and Counterions on the Structures of Silver(I) Complexes: Dominance of Cyclic Dimeric Architecture. *Inorg. Chem.* **2004**, *43*, 6609−6619.

(64) Reger, D. L.; Foley, E. A.; Smith, M. D. Structural Impact of Multitopic Third-Generation Bis(1-Pyrazolyl)Methane Ligands: Double, Mononuclear Metallacyclic Silver(I) Complexes. *Inorg. Chem.* **2010**, *49*, 234−242.

(65) Semeniuc, R. F.; Reger, D. L.; Smith, M. D. Silver(I) and Rhenium(I) Metal Complexes of a 2,2′-Bipyridine-Functionalized Third-Generation Tris(Pyrazolyl)Methane Ligand. *Acta Crystallogr., Sect. C: Struct. Chem.* **2016**, *72*, 826−831.

(66) The τ_4 index can have values between 0 and 1, which corresponds to an ideal square planar or tetrahedral geometry, respectively. (a) Yang, L.; Powell, D. R.; Houser, R. P. Structural Variation in Copper(I) Complexes with Pyridylmethylamide Ligands: Structural Analysis with a New Four-Coordinate Geometry Index, τ_4. *Dalton Trans.* **2007**, *0*, 955−964.

(67) Rosiak, D.; Okuniewski, A.; Chojnacki, J. Novel Complexes Possessing Hg−(Cl, Br, I)···O = C Halogen Bonding and Unusual $Hg_2S_2(Br/I)_4$ Kernel. The Usefulness of τ_4' Structural Parameter. *Polyhedron* **2018**, *146*, 35−41.

(68) A ligand similar to L^{31} was previously reported and complexed with $AgCF_3SO_3$. The $[Ag(L_2)]CF_3SO_3$ complex obtained showed a slightly different structural organization, and no interaction was

present between the iodine and the $CF_3SO_3^-$ anion. (a) Gardinier, J. R.; Hewage, J. S.; Lindeman, S. V. Isomer Dependence in the Assembly and Lability of Silver(I) Trifluoromethanesulfonate Complexes of the Heteroditopic Ligands, 2-, 3-, and 4-[Di(1H-Pyrazolyl)Methyl]Phenyl(Di-p-Tolyl)Phosphine. *Inorg. Chem.* **2014**, *53*, 12108−12121.

(69) Robertson, C. C.; Wright, J. S.; Carrington, E. J.; Perutz, R. N.; Hunter, C. A.; Brammer, L. Hydrogen Bonding vs. Halogen Bonding: The Solvent Decides. *Chem. Sci.* **2017**, *8*, 5392−5398.

(70) The simulated pattern is shifted at higher 2θ values since the SC-XRD measurement is performed at 150 K with respect to the PXRD data collection performed at room temperature.

(71) Mondloch, J. E.; Karagiaridi, O.; Farha, O. K.; Hupp, J. T. Activation of Metal−Organic Framework Materials. *CrystEngComm* **2013**, *15*, 9258−9264.

(72) The normalized distance R^{80} is defined as $R = d(\mathrm{D}\cdots\mathrm{A})/(r_\mathrm{D} + r_\mathrm{A})$ using the Bondi[73] or Alvarez[74] V.d.W radii. See also Brammer et al.[43] for an analogous description. (a) Lommerse, J. P. M.; Stone, A. J.; Taylor, R.; Allen, F. H. The Nature and Geometry of Intermolecular Interactions between Halogens and Oxygen or Nitrogen. *J. Am. Chem. Soc.* **1996**, *118*, 3108−3116.

(73) Bondi, A. Van Der Waals Volumes and Radii. *J. Phys. Chem.* **1964**, *68*, 441−451.

(74) Alvarez, S. A Cartography of the van Der Waals Territories. *Dalton Trans.* **2013**, *42*, 8617−8636.

https://dx.doi.org/10.1021/acs.inorgchem.0c00256